

Dynamics of dual-junction-functionality associative polymer networks with ion and nanoparticle metal-coordinate cross-link junctions

Jake Song, Qiaochu Li, Pangkuan Chen, et al.

Citation: *Journal of Rheology* **66**, 1333 (2022); doi: 10.1122/8.0000410

View online: <https://doi.org/10.1122/8.0000410>

View Table of Contents: <https://sor.scitation.org/toc/jor/66/6>

Published by the [The Society of Rheology](#)

ARTICLES YOU MAY BE INTERESTED IN

[Tailoring the linear viscoelastic response of industrial double dynamics networks through the interplay of associations](#)

Journal of Rheology **66**, 1239 (2022); <https://doi.org/10.1122/8.0000406>

[Relaxation dynamics of supramolecular polymer networks with mixed cross-linkers](#)

Journal of Rheology **66**, 1193 (2022); <https://doi.org/10.1122/8.0000421>

[Rheological investigation on the associative properties of poly\(vinyl alcohol\) solutions](#)

Journal of Rheology **66**, 1141 (2022); <https://doi.org/10.1122/8.0000435>

[Microrheological study of single chain dynamics in semidilute entangled flexible polymer solutions: Crossover from Rouse to Zimm modes](#)

Journal of Rheology **66**, 1165 (2022); <https://doi.org/10.1122/8.0000402>

[Nonlinear shear rheology of single and double dynamics metal-ligand networks](#)

Journal of Rheology **66**, 1223 (2022); <https://doi.org/10.1122/8.0000429>

[A single-chain model for the linear viscoelasticity of unentangled melts of associating polymers](#)

Journal of Rheology **66**, 1183 (2022); <https://doi.org/10.1122/8.0000409>



Advance your science, career
and community as a member of
The Society of Rheology

LEARN MORE





Dynamics of dual-junction-functionality associative polymer networks with ion and nanoparticle metal-coordinate cross-link junctions

Jake Song,^{1,2} Qiaochu Li,¹ Pangkuan Chen,¹ Bavand Keshavarz,² Brian S. Chapman,³ Joseph B. Tracy,³ Gareth H. McKinley,^{2,a)} and Niels Holten-Andersen^{1,b)}

¹*Department of Materials Science and Engineering, Massachusetts Institute of Technology, 77 Massachusetts Avenue, Cambridge, Massachusetts 02139*

²*Hatsopoulos Microfluids Laboratory, Department of Mechanical Engineering, Massachusetts Institute of Technology, 77 Massachusetts Avenue, Cambridge, Massachusetts 02139*

³*Department of Materials Science and Engineering, North Carolina State University, 911 Partners Way, Raleigh, North Carolina 27606*

(Received 2 December 2021; final revision received 15 February 2022; published 1 November 2022)

Abstract

We provide a canonical introduction to dual-junction-functionality associative polymer networks, which combine high and low *functionality* (f) dynamic cross-link junctions to impart load-bearing, dissipation, and self-repairing ability to the network. This unique type of network configuration offers an alternative to traditional dual-junction networks consisting of covalent and reversible cross-links. The high- f junctions can provide load-bearing abilities similar to a covalent cross-link while retaining the ability to self-repair and concurrently confer stimuli-responsive properties arising from the high- f junction species. We demonstrate the mechanical properties of this design motif using metal-coordinating polymer hydrogel networks, which are dynamically cross-linked by different ratios of metal nanoparticle (high- f) and metal ion (low- f) cross-link junctions. We also demonstrate the spontaneous self-assembly of nanoparticle-cross-linked polymers into anisotropic sheets, which may be generalizable for designing dual-junction-functionality associative networks with low volume fraction percolated high- f networks. © 2022 Author(s). All article content, except where otherwise noted, is licensed under a Creative Commons Attribution (CC BY) license (<http://creativecommons.org/licenses/by/4.0/>). <https://doi.org/10.1122/8.0000410>

I. INTRODUCTION

Associative polymer networks have emerged as a popular platform for a growing number of materials applications due to the straightforward control over their viscoelastic properties using different noncovalent cross-linkers [1–5,7,8]. The relaxation time of associative polymer networks can be systematically tuned, primarily by controlling the dissociation rate of the associative species [2,4,6], but also by adjusting the concentration of associative species. The latter change gives rise to a rescaling of the relaxation time (characterizing the numerous dissociation events required to dissociate elastically active polymer strands [7]) and sticky Rouse dynamics (characterizing the constrained Rouse-like dynamics that appear due to the associations between polymer strands [8]). Such systematic insights have enabled the design of advanced soft materials with properties such as injectability [7], self-healing [9,10], and cell compatibility [11]. Studies have also begun to extend these design principles by using *multiple* associative groups within a polymer network, thus

allowing the design of viscoelastic materials with multiple timescales of stress dissipation. Efforts in this area range from utilizing two associating species with different dissociation kinetics to engineer a fast and a slow relaxation response as well as robust damping behavior of the two polymer networks [12–14], to the use of associative species in conjunction with a covalent cross-link to achieve substantially increased toughness in the resulting soft material, predominantly through dissipation mechanisms arising from the transient network created by the associative species [15–17].

Parallel to these developments, there has been a growing exploration of associative networks with cross-linkers of high junction functionality f (which quantifies the total number of associative groups that can be accommodated by an individual cross-linking junction). Representative examples of this approach can be seen in metal-coordination-based associative polymers [18–22], tri-block copolymers [23], ionomers [24], dynamic-covalent colloid-polymer mixtures [25], and hydrophobically modified ethoxylated urethane (HEUR) latex systems [26,27]. Common to high functionality associative networks is a viscoelastic behavior characterized by a slow relaxation of the applied stress in the form of a stretched exponential function, which allows the high functionality networks to retain some of the elastic behavior characteristic of covalent networks, but with a measurable slow relaxation at long times. This mechanical behavior is reminiscent of the

Note: This paper is part of the special issue on Double Dynamics Polymeric Networks

^{a)}Electronic mail: gareth@mit.edu

^{b)}Author to whom correspondence should be addressed; electronic mail: holten@mit.edu

dynamics observed in glassy materials [28] and indicates the presence of a broad distribution of relaxation times resulting from the complex dissociation pathways facilitated by the high- f cross-linker junctions. These characteristics of high junction functionality associative networks make high- f cross-linking junctions promising motifs for engineering the mechanics of soft materials. First, high- f junctions can facilitate a multifold improvement in the stiffness of the associative network compared to low- f junctions. This stiffness enhancement is due to the increase in the network coordination number N , as demonstrated in past studies of metal-coordinate gels [19,20], and illustrated generally by the phantom network theory in which we expect $G \sim k_B T(N - 2)/N$ [29]. Second, high functionality associative networks can serve as load-bearing viscoelastic solids with an ability to self-repair damage through the slow relaxation dynamics mentioned above, and this provides a unique design advantage over covalent networks with permanent junctions that cannot self-repair upon failure or fracture. Finally, networks based on functional high- f junction species can imbue stimuli-responsive properties to the polymer network, such as magneto-responsivity (via magnetic iron oxide nanoparticle junctions) [22] and photo-responsivity (via topology-switching metal-organic cage junctions) [21]. These traits make high- f junctions useful as building blocks for smart and mechanically versatile soft materials. [10,30].

With these advantages in mind, we hypothesized that a *dual-junction-functionality associative polymer network* consisting of fast-relaxing, low- f cross-linker junctions, and slow-relaxing high- f cross-linker junctions can provide the same mechanical attributes as a dual-junction network consisting of fast-relaxing associative junctions and permanent covalent cross-links [15–17], while providing additional desirable properties such as self-repair capability and stimuli-responsivity. In this paper, we describe how such a dual-junction-functionality associative network can be successfully designed through a metal-coordinate polymer network system with fast-relaxing low- f cross-linker junctions (metal ions) and slow-relaxing, high- f cross-linker junctions (metal nanoparticles). We also show that the introduction of nanoparticles into a metal-ion-coordinated associative network results in increasingly solidlike viscoelastic gels at volume fractions far lower than what would be expected from mean-field percolation of polymer-bridged nanoparticles. As observed in earlier work [18], we describe how this early onset of mechanical percolation in the nanoparticle-cross-linked network arises due to the unusual anisotropic self-assembly of the nanoparticle-bridged polymers in the metal-ion-coordinated polymer network. We then demonstrate how this dual-junction–functionality associative network platform can be utilized to optimally design a soft gel that exhibits solidlike responses to tensile deformation on moderate time scales, and yet undergoes spontaneous self-repair of a fractured interface. Our study thus serves as a canonical exploration of the complex but controllable viscoelasticity of dual-junction-functionality associative polymer networks and opens pathways for their adaptation in the future design of soft solidlike materials for stimuli-responsive applications.

II. METHODS

A. Experimental system

The system of choice consists of a four-arm poly(ethylene glycol) polymer end-functionalized with nitrocatechol (4nPEG), and coordinated to either Fe^{3+} ions or Fe_3O_4 nanoparticles (NPs)—a system introduced recently in our prior work [18]. The ions in this configuration act as point cross-linkers with a functionality of $f \leq 3$, while the nanoparticles (of diameter $D = 7$ nm) act as larger cross-link junctions with a maximum possible functionality of $f \sim 100$ based on grafted PEG density estimates performed via dynamic light scattering [22,31]. The addition of both Fe^{3+} ion cross-linkers and NP cross-linkers to a 4nPEG solution thus results in the formation of a network with two types of associative cross-links that contain Fe^{3+} -nitrocatechol coordination interactions, but with markedly different cross-link functionalities f , and thus, very different relaxation timescales. A schematic illustration of the model system configuration is shown in Fig. 1.

Prior to introduction into the polymer network, the nanoparticles are stabilized in water by noncovalent grafting with linear poly(ethylene glycol) chains, which are functionalized on one end with catechol (1cPEG). The catechol ligand facilitates strong binding to the iron surface and allows for excellent aqueous stability of the Fe_3O_4 NPs [31], while being labile enough to be exchanged by nitrocatechol in the 4nPEG. The 4nPEG then binds to the Fe^{3+} sites on the Fe_3O_4 NPs [33] to form a gel network [18]. The reason for the different affinity of catechol and nitrocatechol to the surface of Fe_3O_4 NPs is clarified by the work of Amstad *et al.* who have shown that nitrocatechol can coordinate to Fe^{3+} ions, whereas catechol undergoes oxidative degradation to weaker-binding groups such as quinones and carboxy-containing species [33]. Overall, the NPs act essentially as limited-valency colloids [18,34,35], in which the sterics of the surface-stabilizing 1cPEGs prevents the isotropic association of the NPs and only permits longer-range 4nPEG bridging interactions, and thus, prevents gel collapse through a distinct phase separation as is typically seen in short-range attractive colloids [36].

Our recent work [18] showed that the combination of 4nPEG linkers and NPs give rise to polymer-bridged NP gels, where the morphology and the percolation threshold of the gel could be tuned with careful control of the ratio of the 4nPEG linkers to the number of NPs. Interestingly, it was also shown that adding Fe^{3+} ions to reduce the interaction valency of the NP network—and in doing so, creating a dual network—drastically alters the morphology of this gel, resulting in visible sheetlike 2D nanoparticle-rich lamellar structures in the material, and the percolation of the NP–metal-ion network at volume fractions far below the value observed in the pure NP gel. These findings suggest that, in addition to the benefits associated with the broad relaxation spectrum and superparamagnetic properties of the Fe_3O_4 nanoparticles [22], the addition of the Fe_3O_4 NP high- f junctions to the ion-coordinated polymer network may promote a highly efficient mechanical percolation through anisotropic self-

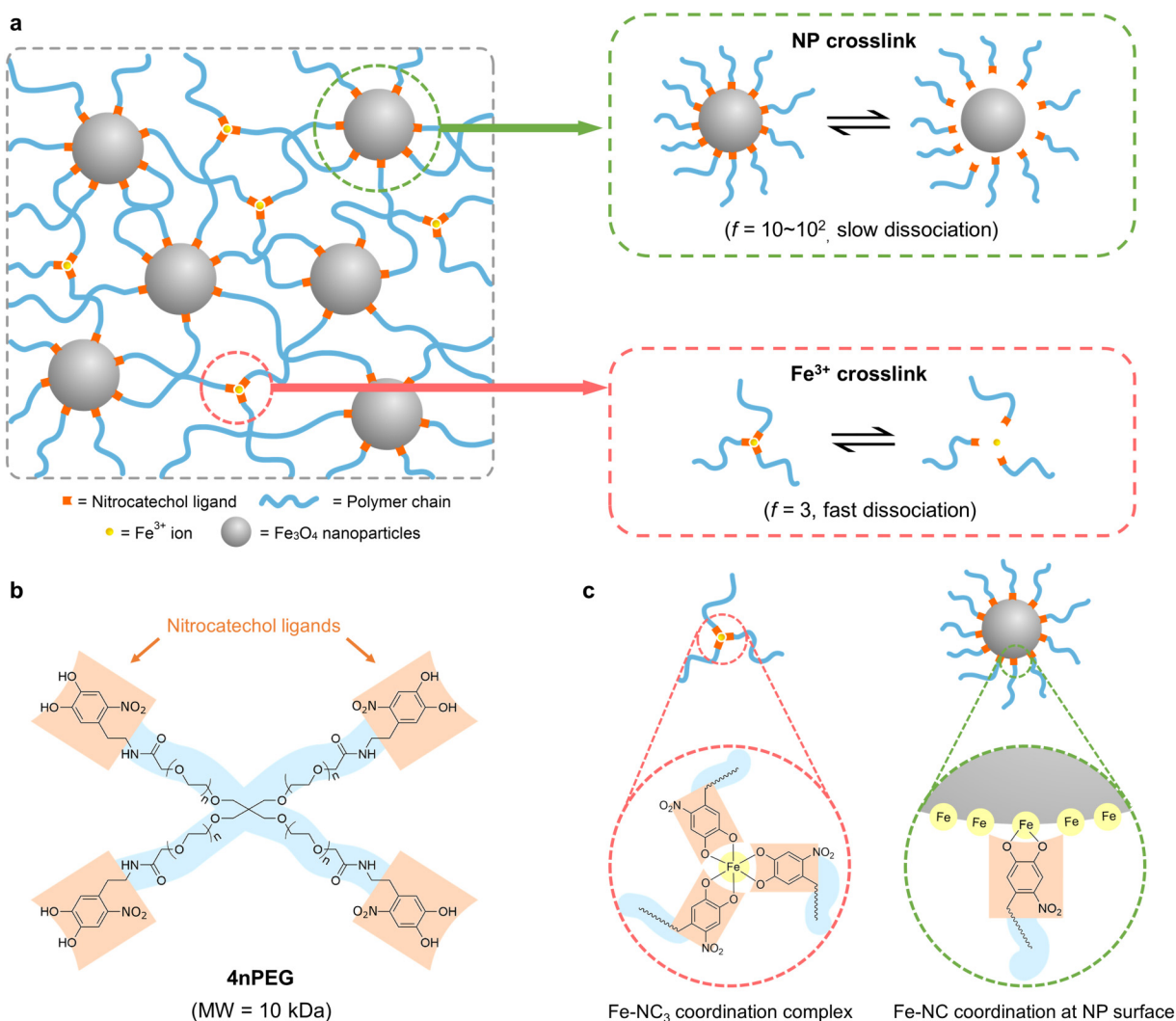


FIG. 1. Dual-functionality metal-coordinate polymer gels with two cross-linking junctions. (a) Schematic illustration of the dual-functionality associative network. Two cross-linking junction motifs are used: Fe³⁺ cross-links which have a fixed junction functionality of $f = 3$ and NP cross-links which have a larger junction functionality of $f \sim 100$. These junctions confer stress relaxation dynamics which are fast and slow, respectively (see Fig. S3) [62]. The NPs (diameter $D = 7$ nm, Fig. S1) [62] are pre-decorated with 1cPEG stabilizers (not drawn in the illustration) as discussed in Sec. II. (b) Molecular structure of the polymer building block 4nPEG, with nitrocatechol (NC) ligands at the chain ends. (c) Chemical structures of the Fe–NC coordination bonds formed at an Fe³⁺ junction and an NP junction, respectively.

assembly. This makes these dual-junction networks—with varying association functionalities, but with the same basic chemistry—a highly promising platform for engineering a wide dynamic range of viscoelastic responses in soft polymeric materials. We extend these aforementioned findings in the recent work and provide practical guidelines for dynamic mechanical applications such as load-bearing and self-repair.

B. Synthesis

1. Reagents

A 4-arm poly(ethylene glycol) bis(acetic acid *N*-succinimidyl) ester (4-NHS-PEG) (MW = 10 kDa) and a mono-functionalized poly(ethylene glycol) bis(acetic acid *N*-succinimidyl) ester (1-NHS-PEG) (MW = 2000 Da) were purchased from JenKem Technology USA, Inc. (Allen, TX). Sodium sulfate (Na₂SO₄), sodium nitrite (NaNO₂), hydrochloric

acid (HCl), dopamine hydrochloride, *N*-methylmorpholine (NMM), 4-(2-hydroxyethyl)-1-piperazineethanesulfonic acid (HEPES), (ethylenedinitrilo)tetraacetic acid (EDTA), methanol (MeOH), ethanol (EtOH), dichloromethane (DCM), *N,N*-dimethylformamide (DMF), diethyl ether (Et₂O), chloroform (CHCl₃), tetrahydrofuran (THF), tetramethylsilane (TMS), dimethyl sulfoxide (DMSO) glutaraldehyde, and oleylamine were purchased from Sigma-Aldrich. Benzyl ether was purchased from Acros Organics. Iron (III) acetylacetonate was purchased from Strem Chemicals. All chemicals were used without further purification.

2. Nitrocatechol ligand

Nitrocatechol is synthesized following reported methods with minor modifications [37]; 1 g dopamine hydrochloride and 1.26 g NaNO₂ are dissolved in 30 ml H₂O. The mixture is stirred and cooled in a salt-ice bath, and 5 ml 20% H₂SO₄

is slowly added dropwise into the mixture upon stirring with the temperature kept below 4 °C. The yellow precipitate that is obtained is washed with cold H₂O three times, cold methanol twice, and cold H₂O twice. Then, the product is mixed with 80 ml H₂O and freeze-dried. The nitro-dopamine hydrogen sulfate product is a yellow powder, with ¹H-NMR (300 MHz, D₂O) δ (ppm): 7.67 (m, 1H, aromatic), 6.87 (m, 1H, aromatic), 3.29 (t, 2H, CH₂ adjacent to -NH₂), 3.17 (t, 2H, CH₂ adjacent to aromatic ring).

3. 1-arm Catechol-functionalized PEG (1cPEG) surfactant

As the surfactant for Fe₃O₄ NP stabilization in an aqueous phase, 1cPEG is synthesized using the reported methods with minor modifications [18]; 228 mg (1.2 mmol) dopamine hydrochloride is neutralized for 15 min with 0.3 ml (2.7 mmol) NMM in 7.5 ml dry DMF under N₂ atmosphere. Then, 1 g (0.5 mmol) 1-NHS-PEG (MW = 2000 Da) dissolved in 7.5 ml DMF is added, and the mixture is stirred with N₂ protection at room temperature for 24 h. The reacted solution is acidified by adding 15 ml 1M HCl (aq), and the product is extracted with CHCl₃ three times. The organic layers are pooled together, dried with NaSO₄, and the solvent is removed by rotary evaporation. Finally, the product concentrate is precipitated in cold Et₂O (-20 °C), filtered, and dried. ¹H NMR (300 MHz, D₂O) δ (ppm): 6.7–6.8 (m, 3H, aromatic), 3.3–4.0 (m, -O-CH₂-CH₂-), 3.4 (t, 2H, CH₂ adjacent to aromatic ring), 2.7 (t, 2H, -CH₂-NH-CO-).

4. 4-arm Nitrocatechol-functionalized PEG (4nPEG)

4nPEG is synthesized using the reported methods with minor modifications [18]; 0.6 mmol nitro-dopamine hydrogen sulfate (178 mg) is neutralized for 15 min with 110 μl (1 mmol) NMM in 4 ml dry DMF under N₂ atmosphere. Then, 1 g (0.1 mmol) 4-NHS-PEG (MW = 10 kDa) dissolved in 4 ml DMF is added, and the mixture is stirred with N₂ protection at room temperature for 24 h. The reacted mixture is mixed with 15 ml 1M HCl (aq), dialyzed with water (MW cut-off = 3500 Da) for 2 days (water exchanged for >5 times), and freeze-dried. ¹H NMR (300 MHz, D₂O) δ (ppm): 7.6 (m, 1H, aromatic), 6.7 (m, 1H, aromatic), 3.6–3.9 (m, -O-CH₂-CH₂-), 3.5 (t, 2H, CH₂ adjacent to aromatic ring), 3.1 (t, 2H, -CH₂-NH-CO-).

5. Fe₃O₄ NPs

Fe₃O₄ NPs are synthesized following the reported methods with minor modifications [18]; 1.05 g of iron (III) acetylacetonate is added to a flask containing a mixture of 15 ml benzyl ether and 15 ml oleylamine. The mixture is stirred and degassed under vacuum at room temperature for 1 h, and heated to 120 °C; the heating ramp rate is 7 °C/min, and at 90 °C, the flask is backfilled with nitrogen. Under inert atmosphere, the flask is held at 120 °C for 1 h, then heated to 210 °C (heating ramp rate 15 °C/min) and held for another 1 h. The flask is cooled to 50 °C and 50 ml of ethanol is added to the mixture. The product is then

centrifuged and dispersed in THF to yield Fe₃O₄ NPs which are functionalized with oleylamine.

6. 1cPEG-functionalized Fe₃O₄ NPs

1cPEG is added to the oleylamine-functionalized Fe₃O₄ NP THF solution at a mass ratio of 3:1 1cPEG/Fe₃O₄. The mixture is heated to 55 °C to facilitate ligand exchange and held for 24 h. The resulting solution is precipitated, washed in hexane thrice, and dried under vacuum. Thermogravimetric (TGA) analysis of the resulting NPs indicates that the mass of the NP core is approximately half of the total mass of the PEGylated-NPs, and this mass of the NP core is used for NP wt. % calculation in each dual gel sample.

7. Preparation of dual-junction-functionality gel networks

75 μl of the 200 mg/ml 4nPEG aqueous (aq) solution is mixed with 25 μl FeCl₃ (aq) solution and 75 μl Fe₃O₄ NP (aq) solution subsequently. The concentrations of FeCl₃ solution and Fe₃O₄ NP solution are based on the desired composition of the dual-junction-functionality gel sample. For example, 80 mM FeCl₃ and 103 mg/ml Fe₃O₄ NP solutions are used to prepare a NP3.5-Fe1 gel. Then, 45 μl 1M HEPES buffer solution (pH = 7.8) is added to raise the pH and induce gelation. The sample is then sealed in a sample mold and cured in a 50 °C oven for 24 h. With different molds, the gel samples can be prepared into specific desired shapes.

8. Preparation of pure Fe³⁺ networks

75 μl of the 200 mg/ml 4nPEG aqueous (aq) solution is mixed with 25 μl 80 mM FeCl₃ (aq) and 45 μl 1M HEPES solution (pH = 7.8). The gel is formed almost immediately after mixing.

9. Preparation of pure NP networks

75 μl of the 200 mg/ml 4nPEG-DMSO solution is mixed with 75 μl of 100 mg (Fe₃O₄ core mass)/ml NP-DMSO solution. The solution mixture was transferred into a mold and sealed, and a solid gel was obtained after curing in a 50 °C oven for 24 hours. The DMSO acts to keep the nitrocatechol in a protonated state, allowing a pure NP gel to be formed by preventing ion extraction through chelation [18]. For these studies, NPs with a diameter $D = 5$ nm, as determined via transmission electron microscopy, were used.

C. Measurements

1. Rheology

All rheological experiments were performed on an Anton Paar MCR-302 rheometer using a smooth parallel plate (diameter = 10 mm) geometry. All tests were done by transferring the gel sample directly to the lower stage of the rheometer. The sample was allowed to equilibrate for 1000 s prior to experiments. A Peltier hood was used for all experiments to control the measurement temperature and prevent solvent evaporation.

Small amplitude oscillatory frequency sweeps of the gels were performed at constant 1% strain and angular frequencies

ranging from 100 to 0.1 rad s⁻¹ on a logarithmic scale while monitoring the storage modulus (G') and loss modulus (G''). Each experiment was performed on three separate samples to ensure reproducibility.

Stress relaxation tests were performed by applying a 2% step strain ($\gamma_0 = 0.02$), and then, the stress $\sigma(t)$ and relaxation modulus $G(t) = \sigma/\gamma_0$ were monitored over time.

2. Transmission and scanning electron microscopy (TEM/SEM)

For TEM imaging of the Fe₃O₄ nanoparticles, a FEI Talos F200X G2 was used. The NPs were dispersed in hexane, and a dilute solution was dropped onto a TEM grid. The size distributions of the NPs were obtained through pixel analysis via IMAGEJ.

For TEM imaging of the gel samples, a FEI Technai Spirit TEM operating at 80 kV was used. The gel samples were first dehydrated by ethanol and propylene oxide, and then, embedded in Embed 812 resin (Electron Microscopy Sciences). The samples were cut with a Reichert Ultracut E ultramicrotome.

For SEM images of the gel samples, a Zeiss Crossbeam 540 FESEM operating at 3–9 kV and 500–1000 pA was used. The gel samples were chemically fixed with 2% glutaraldehyde, and then, dried in a series of EtOH/water solutions of 35, 45, 55, 65, 75, 85, 95, and 100% EtOH. The sample was then dried sequentially in a series of EtOH/TMS mixtures of 50, 20, and 0% EtOH, then air-dried.

3. Tensile tests

Gel specimens for tensile tests were prepared in a dog-bone shaped mold with a gauge length $L = 4.0$ mm, width $w = 1.9$ mm, and thickness $h = 1.4$ mm. To load the gel specimen in the instrument without breaking it by the grips, the grip sections of the dog-bone shaped specimen were bonded to two 18 × 5 mm² acrylic sheets by adhesive. The two acrylic sheets were then held by the grips of the tensile tester to prevent direct gripping on the soft gel samples (see experiment configuration in Fig. S11) [62].

The tensile experiments were performed on a CellScale UStretch mechanical tester with a 0.5 N loadcell. To prevent gel dehydration, a chamber connected to a humidifier was used during the experiments. Unless otherwise indicated, all tensile experiments were performed at a displacement speed of $V = 0.83$ mm/s (corresponding to an initial strain rate of 0.21 s⁻¹ in the gel specimens). Each experiment was performed on three separate specimens to ensure reproducibility.

4. Estimation of the ratio of Fe³⁺ and NP cross-links

Based on the rubber elasticity and transient network theory, the modulus of a gel network is expected to vary as $G' \propto n$, where n is the density of cross-linking bonds [38,39]. Because of the large difference in the relaxation timescales of the Fe³⁺ and NP junction cross-links [18], we are able to approximate the respective contributions of the two cross-linkers to the elasticity of the network in the following manner. At high frequencies such as $\omega = 100$ rad/s, well beyond the cross-over frequency of the Fe³⁺ network

[which corresponds to $\omega_c = 2$ rad/s as shown in Fig. 2(a)], both Fe³⁺ and NP cross-links contribute to the elastic modulus such that $G'(\omega = 100 \text{ rad/s}) \propto n = n_{\text{Fe}^{3+}} + n_{\text{NP}}$. At lower frequencies such as $\omega = 0.3$ rad/s, 98% of the stress carried by the Fe³⁺ cross-links has relaxed due to Fe³⁺ cross-link dissociation [Fig. 2(a)], whereas the NP network still retains almost all of the stress at such frequencies (Fig. S5) [62]. Therefore, for each dual-junction-functionality network, the relative ratio of the numbers of each cross-link can be estimated from small-amplitude oscillatory shear data [Fig. 2(a)] by

$$\frac{n_{\text{NP}}}{n_{\text{total}}} \approx \frac{G'(\omega = 0.3 \text{ rad/s})}{G'(\omega = 100 \text{ rad/s})},$$

$$\frac{n_{\text{Fe}^{3+}}}{n_{\text{total}}} \approx \frac{G'(\omega = 100 \text{ rad/s}) - G'(\omega = 0.3 \text{ rad/s})}{G'(\omega = 100 \text{ rad/s})}.$$

III. RESULTS

A. Linear rheology

We first studied the formation of a dual-junction-functionality network gel by the mixing of 4nPEG, FeCl₃, Fe₃O₄ NPs, and HEPES buffer into a mold, followed by curing at 50 °C overnight. The pH of the resulting hydrogel is ~ 7.4 , which is close to physiological pH and useful for potential applications interfacing with biological tissue. We prepared a series of gel samples with the same 4nPEG concentration (6.8 wt. %), but different concentrations [NP] and [Fe³⁺]. The final composition of each sample is represented as NP x -Fe y , where x is the weight percentage of NPs in the gel, and y is the relative ratio of Fe³⁺ to nitrocatechol (NC) compared to the stoichiometric amount required for tris coordination. For instance, NP3.5-Fe1 refers to a sample with 3.5 wt. % NPs and [Fe³⁺] = 1/3[NC].

The small-amplitude oscillatory shear (SAOS) response of the dual-junction-functionality associative networks is shown in Fig. 2(a). The purely Fe³⁺ ion-coordinated associative gel, NP0-Fe1, exhibits a single mode of stress relaxation governed by the dissociation rate of the metal–ligand pair, in accordance with transient network theories [39,40]. As we add nanoparticles to the system, we observe a noticeable increase in G' at low frequencies (see for instance, NP2.5-Fe1), indicative of mechanical percolation of an NP-based network characterized by a slow and broadly distributed set of relaxation modes [18,22,41]. The emergence of this distinct set of relaxation modes is consistent with prior observations that the NPs preferentially associate with each other, forming an *assortative network* (see sketch in Fig. S12) [42,62]. We propose that the preferential self-assembly of high- f junctions with other high- f junctions, and vice versa, occurs in dual-junction networks with cross-link junctions of varied functionalities (but with the same chemistry) for the following reasons. While the dissociation of polymeric linkers connecting low- f junctions such as metal ions is fast, and therefore, results in fast network rearrangement, the dissociation of polymeric linkers connecting high- f junctions such as NPs can be much slower due to the formation of multivalent polymer linkers between pairs of NPs (i.e., when two NPs are connected by more than one polymer

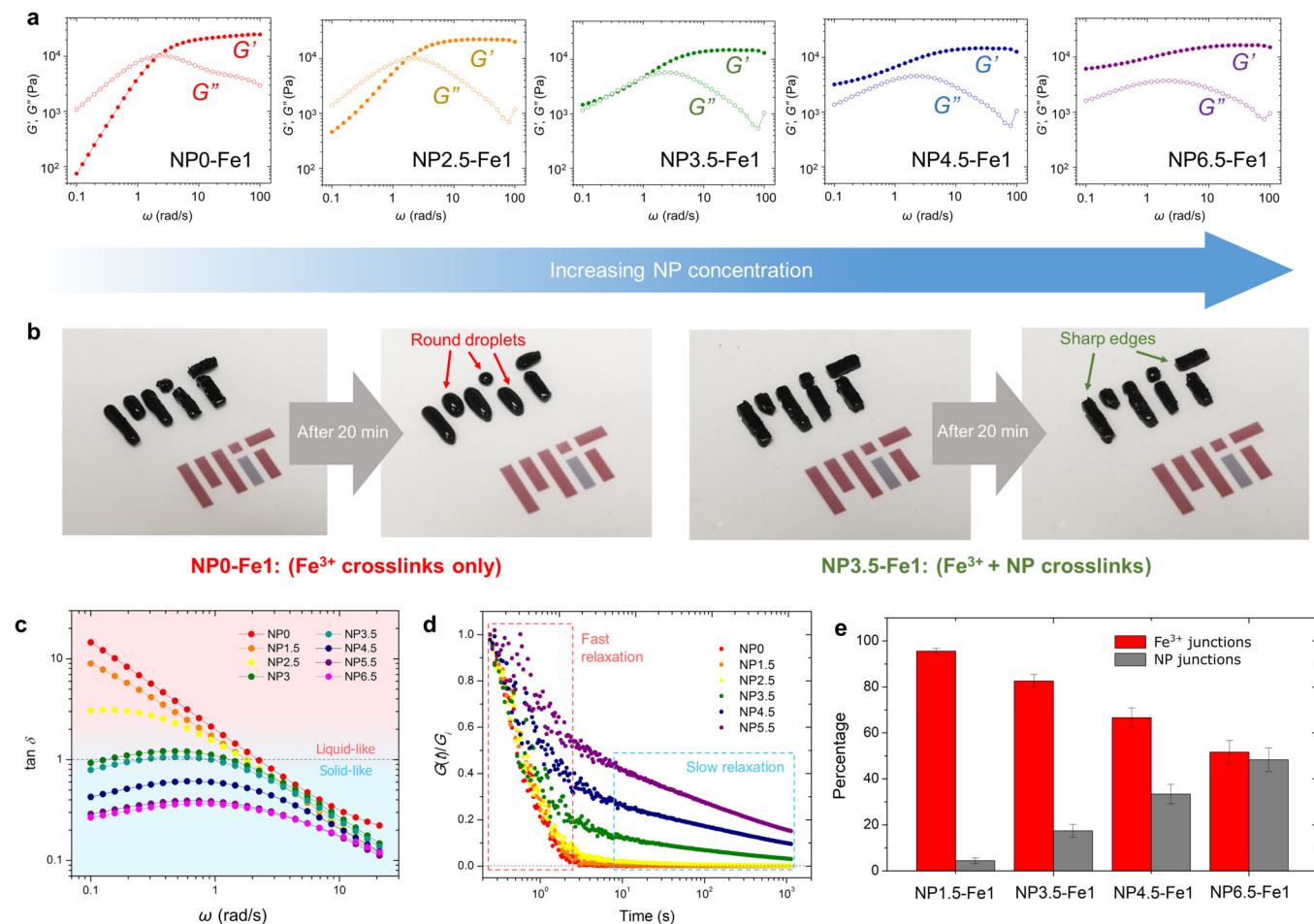


FIG. 2. Linear viscoelastic properties of dual-junction-functionality metal-coordinate networks. (a) Frequency sweeps of the dual-junction-functionality networks, showing a transition from viscoelastic fluid to a soft viscoelastic solid with increasing NP concentrations. (b) Images showing the shape change of a single-junction-functionality Fe^{3+} gel (NP0-Fe1, left) and a dual-junction-functionality gel (NP3.5-Fe1, right) after 20 min. The NP0-Fe1 gel flows into a sessile droplet shape, while the NP3.5-Fe1 gel sustains its solidlike shape and retains sharp edges. (c) $\tan \delta(\omega)$ curves for dual-junction-functionality gel network samples of varied NP concentrations (here, the concentration $[\text{Fe}^{3+}]$ is kept constant as Fe1), showing the transition from a viscoelastic fluid to a viscoelastic solid through the decrease in the phase angle δ at low frequencies. (d) Stress relaxation curves of a series of gel samples with different percentages of nanoparticles (again the concentration $[\text{Fe}^{3+}]$ is kept constant as Fe1), showing fast and slow relaxation processes in two distinct temporal regimes. (e) Percentage of the elastically active polymer chains on the low- f Fe^{3+} cross-link junctions and high- f NP cross-link junctions in dual-junction-functionality gel samples at $\omega = 100$ rad/s at different compositions, estimated from the values of the high-frequency storage modulus $G'(\omega = 100$ rad/s) and low-frequency storage modulus $G'(\omega = 0.3$ rad/s) (see Sec. II).

chain) [26,43,44]. This multivalency results in the kinetically driven self-assembly of high f junctions within dual networks of varied junction functionalities.

Further increase in the concentration of NPs leads to further solidification of the network through an increase in the low frequency elastic modulus. At these high NP concentrations, the hydrogels visibly demonstrate more solidlike characteristics. An example of this is shown in Fig. 2(b), where the NP3.5-Fe1 gel is visually able to sustain a solid shape for at least 20 min, compared to the ion-only gels which behave like a viscoelastic fluid and flows into a surface-energy minimizing droplet shape after 20 min. We quantify the resulting gel solidification occurring as a result of NP network percolation [18,41] by monitoring the evolution in $\tan \delta(\omega) = G''(\omega)/G'(\omega)$, where $\tan \delta = 1$ indicates broadly the transition point between a fluidlike (G'' -dominated) and solidlike (G' -dominated) behavior. As shown in Fig. 2(c), increasing the NP concentration leads to an increasingly solidlike response at low frequencies. We

also find that this fluid–solid transition in the dual-junction associative network can be manipulated by changing the concentration of ions. As we change the concentration of ions in the NP3.5-Fe1 gel, we see that increasing the ion concentration can enhance the dissipative characteristics of the gel, and vice versa (Fig. S2) [62].

We further examined the linear viscoelastic response of the dual-junction-functionality associative networks by performing linear step strain experiments ($\gamma_0 = 2\%$). The resulting stress relaxation of the gels is shown in Fig. 2(d). For comparative purposes, the moduli are normalized by G_i , the initial recorded modulus value at $t = 0$. This plot clearly displays the two distinct relaxation modes of the system—the fast-relaxing Fe^{3+} ion junction and the slow-relaxing Fe_3O_4 NP junction (see Fig. S3 for the corresponding stress relaxation responses of the pure Fe^{3+} ion gel and pure NP gels) [62]. To further demonstrate that these fast and slow relaxation modes arise from low- f ion junctions and high- f NP junctions, respectively, we performed SAOS and stress

relaxation experiments on a gel network immediately after mixing in the NPs, and after 24 h of curing at 50 °C (Fig. S4) [62]. Immediately after mixing in the NPs, the resulting NP4.5-Fe1 gel exhibits a response dominated by the Fe^{3+} ion network, indicated by the presence of a cross-over frequency in small-amplitude oscillatory shear experiments. However, after curing for 24 h, the low frequency elastic modulus increases, the cross-over behavior vanishes, and slow relaxation modes emerge in the network. This trend is consistent with the previously observed slow self-assembly kinetics of the NP-NP percolated network [18], and strongly supports the origin of the slow relaxation modes as arising from high- f NP network junctions. Similarly, we performed an experiment in which we extracted the Fe^{3+} ions from a NP5.0-Fe1 dual-junction network by immersing the gel in EDTA (which chelates the mobile metal ions) for 3 h. The linear viscoelastic response of the resulting gel confirms the expected loss of the low- f junction (fast relaxing) mode following Fe^{3+} ion extraction from a network that now exhibits only the slow relaxation characteristics of a pure high- f junction NP network (Fig. S5) [62].

Since the linear viscoelasticity of the dual-junction-functionality associative network is demonstrably a combination of the temporally distinct relaxation processes of the low and high functionality junctions—a manifestation of the assortative self-assembly of ions and nanoparticles—we

decoupled their respective contributions to the viscoelasticity of the gel networks by comparing the storage modulus of the gel at high- and low-frequency limits of the small-amplitude oscillatory shear data in Fig. 2(a) (see Sec. II for details). The percentage contributions of the storage moduli of the two networks to the overall storage modulus of the system at $\omega = 100$ rad/s are shown in Fig. 2(e).

B. Structure

We have previously shown that contrary to the more isotropic self-assembly of NPs suggested by the sketch in Fig. 1(a), the NPs self-assemble assortatively into anisotropic sheets, thus facilitating a low threshold for mechanical percolation in the dual-junction-functionality network configuration [18]. This is evident in Fig. 2(a) as well, where we see the manifestation of the NP relaxation mode at concentrations as low as 2.5 wt. % NPs—corresponding to a volume fraction of only 0.48 vol. % and much below the percolation threshold of NP-only hydrogels, which can exceed 1 vol. % for NP diameter $D = 7$ nm [18]. To explore the structural origins of this reinforcement behavior, we performed scanning electron microscopy (SEM) on the dual network hydrogel. Figure 3(a) shows SEM micrographs of a dual network with NP5.5-Fe1. In agreement with our recent work [18], we find compelling evidence of the sheetlike anisotropic domains

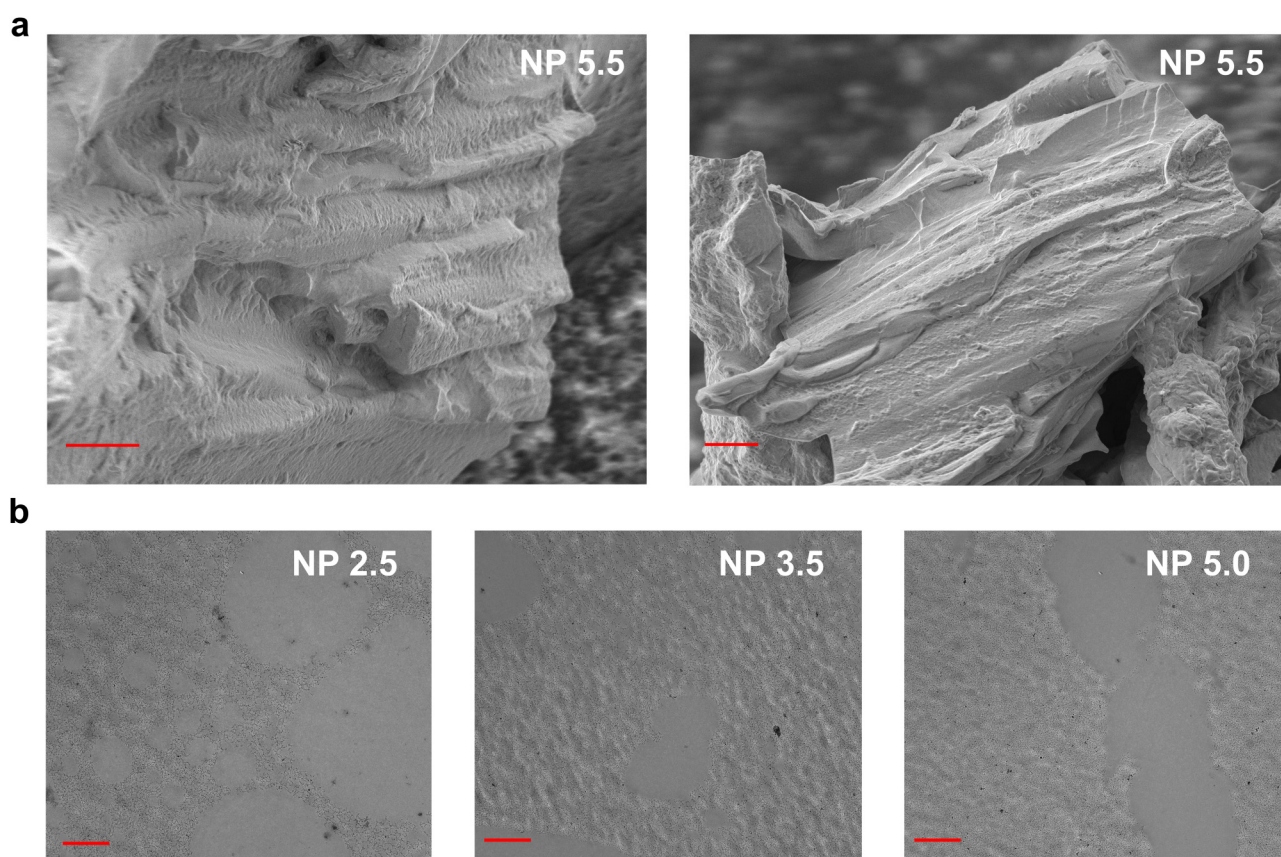


FIG. 3. Internal structure of dual-junction-functionality metal-coordinate networks. (a) Representative scanning electron micrographs of the NP5.5-Fe1 gels; all scale bars: 10 μm . Sheetlike domains are present throughout the samples, intercalated by more amorphous domains. These regions represent NP-rich and NP-poor regions, respectively [18]. (b) Representative transmission electron micrographs of the dual-junction-functionality gels at various NP loadings; all scale bars: 800 nm. Porous nanoparticle assemblies are present at lower NP loadings, which densify with increasing NP concentrations. At higher NP loadings, a microphase separation between NP-rich and NP-poor regions is still present.

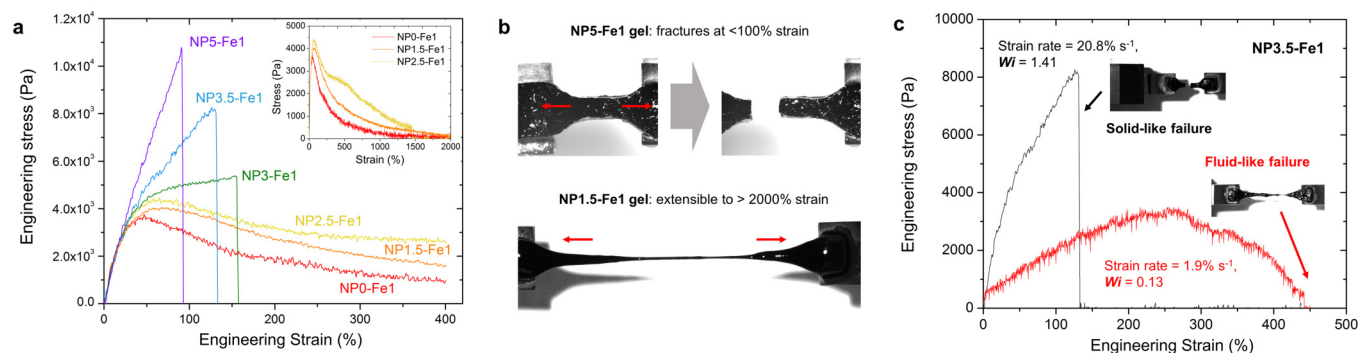


FIG. 4. Tensile properties of dual-junction-functionality metal-coordinate networks. (a) Tensile curves of the dual-junction-functionality gel samples with different compositions are reported in terms of engineering stress and strain. Inset: tensile stress–strain curves of the samples with low NP % extended to large strain (2000%). (b) Images of the failure mode for NP5-Fe1 gel and NP1.5-Fe1 gel (red arrows: stretch directions), showing distinct brittle and ductile failure modes. (c) Tensile curves of the NP3.5-Fe1 gel at two different applied engineering strain rates, with images showing the failure mode in each test.

throughout the sample, intermittently intercalated with amorphous domains. We next performed transmission electron microscopy (TEM) on resin-embedded dual-junction-functionality network hydrogels of increasing NP concentrations to study the internal microstructure of the sheetlike domains. As shown in the micrographs in Fig. 3(b) (higher magnification micrographs can be found in Fig. S1) [62], in the dual-junction-functionality gels of low NP concentrations such as NP2.5-Fe1, the NP-rich regions exhibit significant porosity. In gels of higher NP concentrations such as NP5.5-Fe1, the NP-rich regions become less porous and progressively densify (even though large domains that are NP-rich and NP-poor regions are still present in the NP5.5-Fe1 system). These micrographs show that the high functionality NP junctions self-assemble in a hierarchical manner, forming sparse and porous sheetlike domains in the microstructure that promote the percolation of NP–NP networks at low volume fractions.

The observed sheet formation shares a strong resemblance to what has been observed in (covalently) polymer-grafted nanoparticles (PGNPs). In PGNPs, the sparse and patchy exposed NP interaction sites are understood to facilitate the anisotropic self-assembly of NPs into strings and sheets [45–49], a phenomenon attributed to the small number statistics of the stochastically grafted polymers on the NP structures [47]. The route to self-assembly is slightly different in our NP–NP networks, as we begin with a densely and reversibly grafted system which is well-dispersed in solution, and gradually introduce limited-valency self-assembly through the selective introduction of bridging interactions via nitrocatechol-catechol ligand exchange. Despite these additional effects of the long-range bridging and chemical equilibria which influence the NP–NP self-assembly, our microscopy results in Fig. 3 suggest that the core physics between PGNPs and NP–NP bridging networks may be similar, and that the high-functionality junctions in associative networks can promote self-assembly into striking anisotropic structures through broadly applicable concepts such as the small-number statistics of the binding sites [47]. These findings pose an interesting design opportunity to manipulate the morphology of the anisotropic assemblies of high- f junctions in dual-junction-functionality associative networks, for

example, by taking advantage of their uniquely low volume fraction percolation behavior in load-bearing applications.

C. Non-linear tensile properties of dual-junction-functionality metal-coordinate networks

We next performed uniaxial tensile experiments to complement our linear viscoelastic measurements with non-linear mechanical measurements (see Sec. II for details and Fig. S11 for experimental setup) [62]. Figure 4(a) shows results from the tensile tests of the dual-junction-functionality associative gel samples with different compositions at a crosshead speed of $V = 0.83$ mm/s. Dividing V by the gauge length of $L = 4$ mm gives us an initial strain rate of $\dot{\epsilon} = 0.21$ s $^{-1}$. For the pure Fe $^{3+}$ ion gel with a cross-over frequency of $\omega_c = 2$ rad/s [Fig. 2(a)], and thus, a characteristic relaxation time of $\tau_c = 2\pi/\omega_c = 3.1$ s, this gives us an initial Weissenberg number of $Wi = \tau_c \dot{\epsilon} = 0.62$. However, as the sample elongates at a constant speed and accumulates tensile strain, the strain rate progressively decreases—by the time the samples have been elongated by a factor of four such that the gauge length is $L = 16$ mm, the strain rate becomes $\dot{\epsilon} = 0.05$ s $^{-1}$. For the pure Fe $^{3+}$ ion gel, this gives us a Weissenberg number of $Wi = 0.16$. This evolution of the Weissenberg number with increasing strain provides insights into the tensile stress–strain behavior of the dual-junction-functionality associative gels, especially at lower NP loadings where ductile, fluidlike responses are present.

At low strains, an initial elastic solidlike behavior is observed for all samples studied, with Young’s modulus $E \approx 13$ kPa for all systems. This value is lower than the true Young’s modulus E_p of the system in the limit of high Wi , which can be estimated from the plateau shear modulus of the dual network G_p by using the high-frequency shear modulus $G'(\omega = 100$ rad/s) ≈ 20 kPa and the relation $E_p = 2G_p(1 + \nu)$. A Poisson’s ratio of $\nu = 0.5$ leads to a prediction of the plateau Young’s modulus to be as high as $E_p \approx 60$ kPa. The discrepancy in the measured moduli from this asymptotic value can be accounted for by the partial relaxation of the Fe $^{3+}$ cross-link junctions at the low imposed strain rate being considered here ($\dot{\epsilon} = 0.21$ s $^{-1}$).

At higher axial strains, there is a systematic difference in the stress-strain curves of the gels with different nanoparticle concentrations. For the pure Fe^{3+} ion gel (NP0-Fe1), a ductile, fluidlike flow behavior can be observed, which is characterized by a slow decay in the stress over large strains. This can be understood with reference to the viscoelastic characteristics of the gel sample, as discussed by Malkin and Petrie, in which elongated polymeric specimens no longer show solidlike cohesive failure and instead begin to undergo ductile, liquidlike flow at $Wi < 0.5$ [50]. At slightly higher NP loadings such as our NP1.5-Fe1 and NP2.5-Fe1 gels, we still observe such flow behaviors but with higher stress values—and this can be understood through the framework described by Guth and Gold [51], as arising from the mechanical reinforcement provided by the NPs dispersed in the polymer matrix. At even higher NP loadings, mechanical percolation of the NP network occurs [Fig. 2(a)], and this results in a dramatic increase in the effective relaxation time of the percolated system over what can be achieved using Fe^{3+} ion junctions alone. A stretched exponential fit to the stress relaxation data for the pure NP gel (shown in Fig. S3) [62] yields a characteristic relaxation time value of $\tau_c = 1.6 \times 10^4$ s, a value dramatically larger than the relaxation time of the pure ion network ($\tau_c = 3.1$ s). The Weissenberg number is thus significantly higher in dual gels with higher NP loadings, resulting in the elimination of ductile fluidlike elongation behavior, and the emergence of solidlike stress-strain curves characterized by a cohesive failure at finite strains, and eventually, a completely brittle response with nearly-linear stress-strain curve and very small failure strains, as observed in the NP5-Fe1 gel.

The different failure modes of these gels are captured in Fig. 4(b); the NP1.5-Fe1 gel yields at $\sim 50\%$ strain and can be further stretched into a thin filament with $>2000\%$ strain, showing a ductile necking failure, whereas the NP5-Fe1 gel undergoes brittle failure at $<100\%$ strain with distinct fracture surfaces. For the samples with intermediate NP concentrations, there is a clear transition of tensile behavior between the two extremes. For instance, the NP3.5-Fe1 sample behaves initially like an elastic solid but with some softening beyond 50% strain, as shown in Fig. 4(a). This sample also exhibits repeatable hysteresis in the cyclic tensile experiments, showing significant energy dissipation due to the highly dynamic nature of the dual-functionality junctions (see Fig. S6a) [62]. The Weissenberg number dependence of the mechanical properties of these dual-junction-functionality networks is further demonstrated in Fig. 4(c), where we study the response of the NP3.5-Fe1 gel under different strain rates and observe a transition between a stiffer solidlike response at the higher strain rate and a more dissipative ductile response at the lower strain rate. The cross-over frequency of the NP3.5-Fe1 gel is approximately $\omega_c = 0.92$ rad/s, thus giving an estimated relaxation time of $\tau_c = 2\pi/\omega_c = 6.8$ s. Combining this with an imposed cross-head speed of $V = 0.83$ mm/s and a sample gauge length of $L = 4$ mm, we obtain an initial Weissenberg number of $Wi = 1.41$, at which the material exhibits cohesive solidlike failure; whereas at the slower speed of $V = 0.08$ mm/s, the Weissenberg number decreases to $Wi = 0.13$, resulting in the ductile fluidlike response discussed earlier. The progressive

emergence of this fluidlike behavior with decreasing strain rate is illustrated in greater detail in Fig. S6b [62].

The stress-strain curves in Fig. 4(a) indicate that there is an optimal concentration of nanoparticles at which we can maximize the toughness of the system. As shown in Fig. S7 [62], the toughness of the dual network (defined here as the area under the stress-strain curve) initially increases with the nanoparticle concentration due to filler reinforcement. The toughness is shown to peak at a composition of NP2.5-Fe1 (for the studied tensile deformation rate of $V = 0.83$ mm/s). The toughness then decreases at higher nanoparticle concentrations, due to the increasingly stiff elastic behavior of the system *en route* to brittle failure at a very high Weissenberg number. Interestingly, Fig. S7 [62] also shows that even though the NP5-Fe1 gel exhibits brittle failure, it has a higher toughness than the pure NP gel at the same NP loading. These promising results are reminiscent of rubber-toughening mechanisms in filled composites, and indicate that dual-junction-functionality associative networks with high- f junctions may exhibit toughness-enhancing mechanisms similar to those that have been demonstrated in dual networks with covalent and reversible bonds [15,17,52]. A more comprehensive exploration of this idea is beyond the scope of the current work as this would require a large number of samples to facilitate stress-strain analysis over multiple strain rates and Weissenberg numbers, as well as a careful determination of the fracture energies.

D. Self-adhesion

Finally, we reasoned that these unique dynamic properties of the dual-junction-functionality networks could be harnessed to design gels that are simultaneously load-bearing and self-repairing. We can expect such repair to occur in our gels through a mechanism of self-adhesion [30,53]—in which two equilibrium interfaces of a previously cleaved surface will undergo re-adhesion when placed back in contact through the re-equilibration and relaxation of polymer strands, and thereby facilitate the repair of a macroscopic gel sample. To simultaneously attain load-bearing and self-repair, a combination of slow and fast relaxation dynamics (via high- f and low- f cross-link junctions) is required. Indeed, in a typical cut-and-adhere experiment, a pure Fe^{3+} ion gel can self-repair within 1 min (Fig. S8a) [62] due to its viscoelastic fluidlike response characteristics, but cannot bear stress over experimentally-relevant timescales as a result, whereas a pure NP gel can bear load as a stiff self-supporting elastic solid, but cannot self-repair after a fracture over experimentally-relevant timescales due to the very slow NP cross-link dynamics (Fig. S8b) [62].

Thus, we reasoned that a gel system with optimized numbers of high- f and low- f cross-link junctions may be able to achieve both properties, simultaneously. To demonstrate this, we select the NP3.5-Fe1 gel, which has a loss tangent value of $\tan\delta \approx 1$ below the expected cross-over frequency of the pure ion gel at $\omega_c = 2$ rad/s [Fig. 2(c)], indicating almost equal contributions of elastic solidlike and viscous liquidlike characteristics in the material. As shown in Fig. 5(a) and illustrated in 5(b), fracturing the NP3.5-Fe1 gel

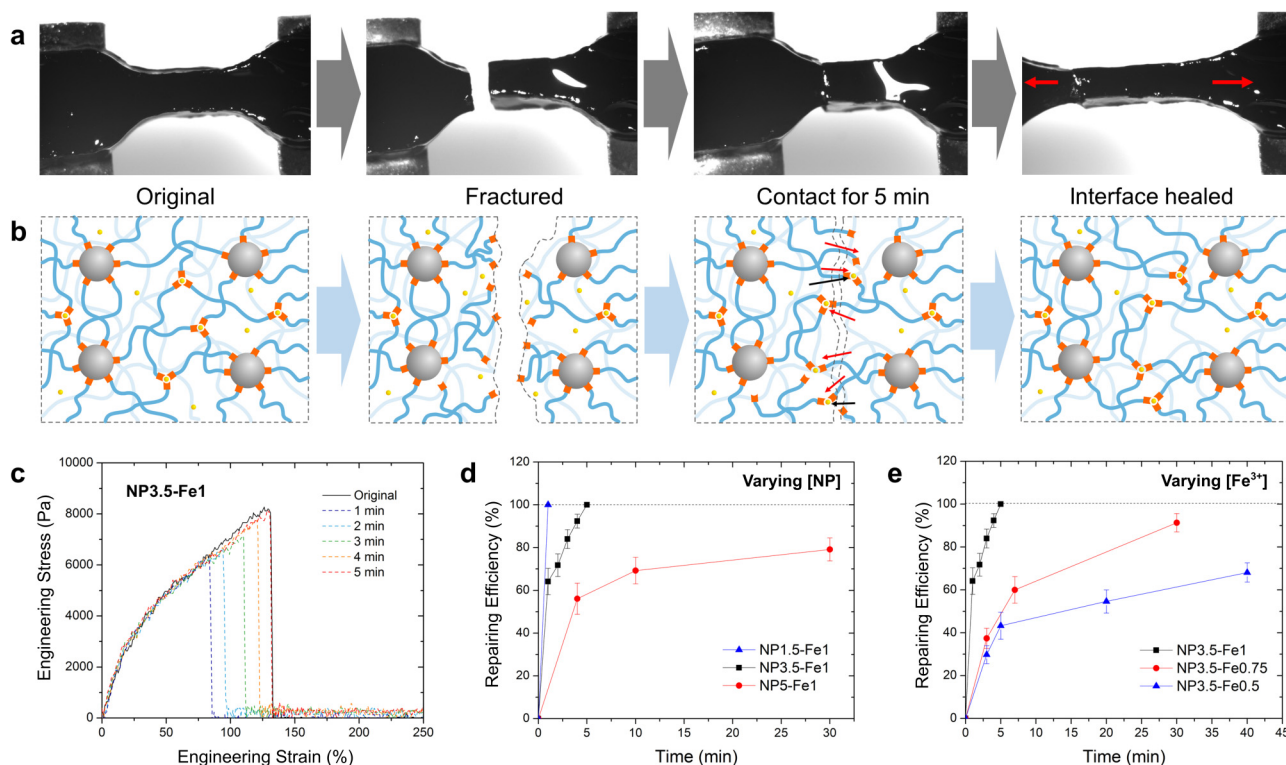


FIG. 5. Self-repair of the fractured interfaces in dual-junction-functionality metal-coordinate networks. (a) Images of the fracture and rapid self-adhesion process for a NP3.5-Fe1 gel sample, and (b) schematic illustration of the proposed repair mechanism at each stage. (c) Tensile curves of a NP3.5-Fe1 sample before fracture and after self-repair for different lengths of contact adhesion time. (d) Repair efficiency profiles of the hybrid gel samples with different NP concentrations and (e) with different Fe³⁺ concentrations.

sample and putting the fractured surfaces back into contact leads to effective autonomous self-repair without any external stimuli. Tensile experiments confirm that by self-repairing for 5 min under ambient conditions, the NP3.5-Fe1 gel can fully recover its original mechanical property as shown in Fig. 5(c). These self-repair rates are notable, since reported self-repair times of the hydrogels of similar stiffness ($>10^4$ Pa) often need hours or even days to fully recover [54–56], and many of them (especially with covalent bonds) require external triggers, such as heating, light stimuli or addition of solvents [57–59]. We also anticipate that the self-adhering kinetics in our system would be accelerated by bringing the fractured interface back into contact more rapidly (within the relaxation time τ_c), which would increase the abundance of open (unbonded) stickers at the interface, reduce the self-adhesion time even further, and potentially transition into a fully self-healing material regime [53].

Changing the ratios of the low- f ion junctions and high- f NP junctions also affects the self-repairing ability of the network, as shown in Figs. 5(d) and 5(e). We define a self-repairing efficiency $\eta = \frac{\epsilon_{\text{healed}}}{\epsilon_{\text{original}}} \times 100\%$, where $\epsilon_{\text{original}}$ and ϵ_{healed} are the maximum tensile strain achieved in the material before and after fracture in the self-adhesion test. We conduct these tests on dual-junction-functionality gel samples with different ion and NP compositions (see tensile curves in Fig. S9) [62] and plot their self-adhesion efficiencies as a function of time. In all of these self-adhesion-based material property recovery profiles, there is a quick initial recovery in

the first few minutes with greater than 40% recovery in the property, suggesting that fast ion-governed relaxation processes drive the rapid initial rearrangement of the network across the two interfaces. The overall recovery efficiency drops with the increasing ratio of NP to Fe³⁺ ions in the dual-junction-functionality network as shown in Figs. 5(d) and 5(e). These trends are consistent with the expected effect of the changing ratio of load-bearing junctions characterized in Fig. 2(e), i.e., the self-adhesion rate achieved in the NP-NP network is much slower owing to the slower rearrangement of the NP-NP network [Fig. 2(d), S3] [62]. In agreement with this interpretation, we observed that the healing rate of the NP-NP network can be accelerated by thermal equilibration as qualitatively demonstrated in Fig. S10 [62].

Overall, the fast-dissociating Fe³⁺ cross-links provide a fast initial flow that facilitates intimate contact between the two fractured interfaces as well as diffusion of the polymeric components in the metal ion network for rapid initial network recovery, while the slowly dissociating high-functionality NP cross-links form a stiff elastic scaffold to sustain a solid shape—in a similar vein to covalent-bond-based dual networks [15–17]. Here, we have shown that the percolation state of the NP cross-links can be manipulated to engineer a dual-junction-functionality viscoelastic gel which exhibits different extents of solidlike characteristics and self-repairing capabilities as shown in Figs. 4 and 5. We also show that there is an optimal percolation state of the NPs

(NP3.5-Fe1, which is close to a critical gel with $\tan \delta \sim 1$ over a wide range of frequencies) in which both load-bearing and self-repair capabilities are observed within experimental timeframes. We note that the use of these high- f junctions offers a considerable advantage over covalent junctions, as the high- f junctions have a long but finite characteristic relaxation time, which, unlike covalently-bonded gels can be further tuned by temperature. In other words, equilibrating the NP-rich dual-junction gel or pure NP gel at high temperatures (which might be generated, for example, via inductive heating) still allows for the self-adhesion of the dual gel network even in the absence of the mobile Fe^{3+} junctions (Fig. S10) [62], in contrast to pure covalent gels which cannot recover after failure. We thus anticipate that these dual-junction–functionality associative networks will facilitate the design of responsive gels with increased toughness, while maintaining self-repairing abilities in a manner that is superior to covalent-based dual networks.

V. DISCUSSION AND CONCLUSION

This work lays the foundation for utilizing dual-junction–functionality associative networks (consisting of fast-relaxing low-functionality junctions and slower high-functionality cross-linker junctions) in diverse soft material science applications. We have investigated the linear and nonlinear mechanics of such networks constructed via nitrocatechol coordination to Fe^{3+} ions (low functionality junctions) and Fe_3O_4 nanoparticles (high functionality junctions), and have shown that an optimal balance of the high- f and low- f junctions can yield a load-bearing and self-adhering gel which is tougher than either of the individual constituents (i.e., ion-only and NP-only gels). The high- f Fe_3O_4 NP junction represents a particularly attractive motif for replacing covalent moieties in traditional dual networks [15–17], as the resulting NP networks display a measurable relaxation time, and therefore, confer self-repairing properties to elastic solid-like gels at room temperature without necessitating external stimuli [57–59], while also offering responsive functionalities such as magnetoresponsivity and photoresponsivity [19,21,22]. Our findings in these model systems (in which both networks are based on the same Fe-nitrocatechol associative chemistry and differ only in the junction functionality) should also apply generally to other dual-functionality associative networks such as latex-HEUR systems [60], as well as dual-functionality associative networks constructed via high- f junctions in locally glassy spherical domains [23,61], metal-organic cages [20], or precisely engineered colloids [25].

The unusual self-assembly of the nanoparticles in the form of anisotropic sheets (and the resulting earlier onset of mechanical percolation) observed in this work and our earlier study [18] remains intriguing and warrants additional studies. Elucidating whether these anisotropic assemblies are a result of the specific construction of our system (for example, the pre-grafting of the NPs with stabilizing polymers) or whether they are also applicable to other high-functionality junctions simply as a result of small-number statistics [47] may open design opportunities to create dual-junction associative

networks with highly efficient mechanical reinforcement properties at a low volume fraction of fillers. Moreover, elucidating the domain size of these anisotropic assemblies and extending the size of such assemblies to macroscopic scales could also open windows to designing dual networks with macroscopically anisotropic structure and mechanical properties, and create novel methods of designing functional gel materials.

ACKNOWLEDGMENTS

We acknowledge financial support from the National Science Foundation via Grant Nos. CBET-1605943 and CBET-1605699, and the Army Research Office through the Institute for Soldier Nanotechnologies at MIT via Contract No. W911NF-13-D-0001. We acknowledge instrumental access at the W.M. Keck Foundation Biological Imaging Facility at the Whitehead Institute, and the Nanotechnology Materials Facility at the Koch Institute. We thank Nicki Watson and David Mankus for their help in the TEM and SEM characterizations at these respective facilities. J.S. would like to acknowledge helpful conversations with S. Kumar (Columbia University), H. Le Roy (Univ. Paris-Sud), and B. Lynch (North Carolina State University).

AUTHOR DECLARATIONS

Conflict of Interest

The authors declare no conflict of interests.

Author Contributions

J.S. and Q.L. contributed equally to this work.

REFERENCES

- [1] Rubinstein, M., and A. V. Dobrynin, "Solutions of associative polymers," *Trends Polym. Sci.* **5**, 181–186 (1997).
- [2] Zhang, Z., Q. Chen, and R. H. Colby, "Dynamics of associative polymers," *Soft Matter* **14**, 2961–2977 (2018).
- [3] Golkaram, M., and K. Loos, "A critical approach to polymer dynamics in supramolecular polymers," *Macromolecules* **52**, 9427–9444 (2019).
- [4] Yount, W. C., D. M. Loveless, and S. L. Craig, "Strong means slow: Dynamic contributions to the bulk mechanical properties of supramolecular networks," *Angew. Chem. Int. Ed.* **44**, 2746–2748 (2005).
- [5] Marco-Dufort, B., R. Iten, and M. W. Tibbitt, "Linking molecular behavior to macroscopic properties in ideal dynamic covalent networks," *J. Am. Chem. Soc.* **142**, 15371–15385 (2020).
- [6] Tanaka, F., and S. F. Edwards, "Viscoelastic properties of physically crosslinked networks: Part 2. Dynamic mechanical moduli," *J. Non-Newtonian Fluid Mech.* **43**, 273–288 (1992).
- [7] Rubinstein, M., and A. N. Semenov, "Thermoreversible gelation in solutions of associating polymers. 2. Linear dynamics," *Macromolecules* **31**, 1386–1397 (1998).
- [8] Chen, Q., G. J. Tudryn, and R. H. Colby, "Ionomer dynamics and the sticky rouse model," *J. Rheol.* **57**, 1441–1462 (2013).
- [9] Kang, J., J. B.-H. Tok, and Z. Bao, "Self-healing soft electronics," *Nat. Electron.* **2**, 144–150 (2019).
- [10] Tan, Y. J., G. J. Susanto, H. P. Anwar Ali, and B. C. K. Tee, "Progress and roadmap for intelligent self-healing materials in autonomous robotics," *Adv. Mater.* **33**, 2002800 (2021).

- [11] Rosales, A. M., and K. S. Anseth, "The design of reversible hydrogels to capture extracellular matrix dynamics," *Nat. Rev. Mater.* **1**, 1–15 (2016).
- [12] Grindy, S. C., R. Learsch, D. Mozhdzhi, J. Cheng, D. G. Barrett, Z. Guan, P. B. Messersmith, and N. Holten-Andersen, "Control of hierarchical polymer mechanics with bioinspired metal-coordination dynamics," *Nat. Mater.* **14**, 1210–1216 (2015).
- [13] Zhang, R., C. Zhang, Z. Yang, Q. Wu, P. Sun, and X. Wang, "Hierarchical dynamics in a transient polymer network cross-linked by orthogonal dynamic bonds," *Macromolecules* **53**, 5937–5949 (2020).
- [14] Loveless, D. M., S. L. Jeon, and S. L. Craig, "Rational control of viscoelastic properties in multicomponent associative polymer networks," *Macromolecules* **38**, 10171–10177 (2005).
- [15] Filippidi, E., T. R. Cristiani, C. D. Eisenbach, J. H. Waite, J. N. Israelachvili, B. K. Ahn, and M. T. Valentine, "Toughening elastomers using mussel-inspired iron-catechol complexes," *Science* **358**, 502–505 (2017).
- [16] Mayumi, K., A. Marcellan, G. Ducouret, C. Creton, and T. Narita, "Stress-strain relationship of highly stretchable dual cross-link gels: Separability of strain and time effect," *ACS Macro Lett.* **2**, 1065–1068 (2013).
- [17] Mayumi, K., J. Guo, T. Narita, C. Y. Hui, and C. Creton, "Fracture of dual crosslink gels with permanent and transient crosslinks," *Extreme Mech. Lett.* **6**, 52–59 (2016).
- [18] Song, J., M. H. Rizvi, B. B. Lynch, J. Ilavsky, D. Mankus, J. B. Tracy, G. H. McKinley, and N. Holten-Andersen, "Programmable anisotropy and percolation in supramolecular patchy particle gels," *ACS Nano* **14**, 17018–17027 (2020).
- [19] Kim, S., A. U. Regitsky, J. Song, J. Ilavsky, G. H. McKinley, and N. Holten-Andersen, "In situ mechanical reinforcement of polymer hydrogels via metal-coordinated cross-link mineralization," *Nat. Commun.* **12**, 667 (2021).
- [20] Zhukhovitskiy, A. V., M. Zhong, E. G. Keeler, V. K. Michaelis, J. E. P. Sun, M. J. A. Hore, D. J. Pochan, R. G. Griffin, A. P. Willard, and J. A. Johnson, "Highly branched and loop-rich gels via formation of metal-organic cages linked by polymers," *Nat. Chem.* **8**, 33–41 (2016).
- [21] Gu, Y., E. A. Alt, H. Wang, X. Li, A. P. Willard, and J. A. Johnson, "Photoswitching topology in polymer networks with metal-organic cages as crosslinks," *Nature* **560**, 65–69 (2018).
- [22] Li, Q., D. G. Barrett, P. B. Messersmith, and N. Holten-Andersen, "Controlling hydrogel mechanics via bio-inspired polymer-nanoparticle bond dynamics," *ACS Nano* **10**, 1317–1324 (2016).
- [23] Erk, K. A., and K. R. Shull, "Rate-dependent stiffening and strain localization in physically associating solutions," *Macromolecules* **44**, 932–939 (2011).
- [24] Chen, Q., S. Liang, H.-S. Shiao, and R. H. Colby, "Linear viscoelastic and dielectric properties of phosphonium siloxane ionomers," *ACS Macro Lett.* **2**, 970–974 (2013).
- [25] Dominguez, M. N. *et al.*, "Assembly of linked nanocrystal colloids by reversible covalent bonds," *Chem. Mater.* **32**, 10235–10245 (2020).
- [26] Wang, S., and R. G. Larson, "Multiple relaxation modes in suspensions of colloidal particles bridged by telechelic polymers," *J. Rheol.* **62**, 477–490 (2018).
- [27] Hajizadeh, E., S. Yu, S. Wang, and R. G. Larson, "A novel hybrid population balance–Brownian dynamics method for simulating the dynamics of polymer-bridged colloidal latex particle suspensions," *J. Rheol.* **62**, 235–247 (2018).
- [28] Phillips, J., "Stretched exponential relaxation in molecular and electronic glasses," *Rep. Prog. Phys.* **59**, 1133–1207 (1996).
- [29] Rubinstein, M., and R. H. Colby, *Polymer Physics* (Oxford University, NY, 2003), Vol. 23.
- [30] Campanella, A., D. Döhler, and W. H. Binder, "Self-healing in supramolecular polymers," *Macromol. Rapid Commun.* **39**, 1700739 (2018).
- [31] Amstad, E., T. Gillich, I. Bilecka, M. Textor, and E. Reimhult, "Ultrastable iron oxide nanoparticle colloidal suspensions using dispersants with catechol-derived anchor groups," *Nano Lett.* **9**, 4042–4048 (2009).
- [32] Holten-Andersen, N., M. J. Harrington, H. Birkedal, B. P. Lee, P. B. Messersmith, K. Y. C. Lee, and J. H. Waite, "pH-induced metal-ligand cross-links inspired by mussel yield self-healing polymer networks with near-covalent elastic moduli," *Proc. Natl. Acad. Sci. USA* **108**, 2651–2655 (2011).
- [33] Amstad, E., A. U. Gehring, H. Fischer, V. V. Nagaiyanallur, G. Hähner, M. Textor, and E. Reimhult, "Influence of electronegative substituents on the binding affinity of catechol-derived anchors to Fe₃O₄ nanoparticles," *J. Phys. Chem. C* **115**, 683–691 (2011).
- [34] Zaccarelli, E., "Colloidal gels: Equilibrium and non-equilibrium routes," *J. Phys. Condens. Matter* **19**, 323101 (2007).
- [35] Lindquist, B. A., R. B. Jadrich, D. J. Milliron, and T. M. Truskett, "On the formation of equilibrium gels via a macroscopic bond limitation," *J. Chem. Phys.* **145**, 074906 (2016).
- [36] Lu, P. J., E. Zaccarelli, F. Ciulla, A. B. Schofield, F. Sciortino, and D. A. Weitz, "Gelation of particles with short-range attraction," *Nature* **453**, 499–503 (2008).
- [37] Shafiq, Z., J. Cui, L. Pastor-Pérez, V. San Miguel, R. A. Gropeanu, C. Serrano, and A. del Campo, "Bioinspired underwater bonding and debonding on demand," *Angew. Chem.* **124**, 4408–4411 (2012).
- [38] Treloar, L. R. G., *The Physics of Rubber Elasticity* (Oxford University Press, New York, NY, 1975).
- [39] Tanaka, F., and S. F. Edwards, "Viscoelastic properties of physically crosslinked networks. 1. Transient network theory," *Macromolecules* **25**, 1516–1523 (1992).
- [40] Annable, T., R. Buscall, R. Ettelaie, and D. Whittlestone, "The rheology of solutions of associating polymers: Comparison of experimental behavior with transient network theory," *J. Rheol.* **37**, 695–726 (1993).
- [41] Akcora, P. *et al.*, "'Gel-like' mechanical reinforcement in polymer nanocomposite melts," *Macromolecules* **43**, 1003–1010 (2010).
- [42] Newman, M. E. J., "Assortative mixing in networks," *Phys. Rev. Lett.* **89**, 208701 (2002).
- [43] Gomez-Casado, A., H. H. Dam, M. D. Yilmaz, D. Florea, P. Jonkheijm, and J. Huskens, "Probing multivalent interactions in a synthetic host-guest complex by dynamic force spectroscopy," *J. Am. Chem. Soc.* **133**, 10849–10857 (2011).
- [44] Huskens, J., L. J. Prins, R. Haag, and B. J. Ravoo, *Multivalency Concepts, Research and Applications* (Wiley, Hoboken, NJ, 2018).
- [45] Akcora, P. *et al.*, "Anisotropic self-assembly of spherical polymer-grafted nanoparticles," *Nat. Mater.* **8**, 354–359 (2009).
- [46] Kumar, S. K., N. Jouault, B. Benicewicz, and T. Neely, "Nanocomposites with polymer grafted nanoparticles," *Macromolecules* **46**, 3199–3214 (2013).
- [47] Bozorgui, B., D. Meng, S. K. Kumar, C. Chakravarty, and A. Cacciuto, "Fluctuation-driven anisotropic assembly in nanoscale systems," *Nano Lett.* **13**, 2732–2737 (2013).
- [48] Asai, M., A. Cacciuto, and S. K. Kumar, "Quantitative analogy polymer-grafted nanoparticles and patchy particles," *Soft Matter* **11**, 793–797 (2015).
- [49] Chremos, A., and J. F. Douglas, "Self-assembly of polymer-grafted nanoparticles in solvent-free conditions," *Soft Matter* **12**, 9527–9537 (2016).
- [50] Malkin, A. Y., and C. J. S. Petrie, "Some conditions for rupture of polymer liquids in extension," *J. Rheol.* **41**, 1–25 (1997).

- [51] Guth, E., "Theory of filler reinforcement," *J. Appl. Phys.* **16**, 20–25 (1945).
- [52] Creton, C., "50th anniversary perspective: Networks and gels: Soft but dynamic and tough," *Macromolecules* **50**, 8297–8316 (2017).
- [53] Stukalin, E. B., L.-H. Cai, N. A. Kumar, L. Leibler, and M. Rubinstein, "Self-healing of unentangled polymer networks with reversible bonds," *Macromolecules* **46**, 7525–7541 (2013).
- [54] Imato, K., M. Nishihara, T. Kanehara, Y. Amamoto, A. Takahara, and H. Otsuka, "Self-healing of chemical gels cross-linked by diarylbibenzofuranone-based trigger-free dynamic covalent bonds at room temperature," *Angew. Chem. Int. Ed.* **51**, 1138–1142 (2012).
- [55] Yu, C., C.-F. Wang, and S. Chen, "Robust self-healing host–guest gels from magnetocaloric radical polymerization," *Adv. Funct. Mater.* **24**, 1235–1242 (2014).
- [56] Zhang, H., H. Xia, and Y. Zhao, "Poly (vinyl alcohol) hydrogel can autonomously self-heal," *ACS Macro Lett.* **1**, 1233–1236 (2012).
- [57] Gulyuz, U., and O. Okay, "Self-healing poly (acrylic acid) hydrogels with shape memory behavior of high mechanical strength," *Macromolecules* **47**, 6889–6899 (2014).
- [58] Amamoto, Y., J. Kamada, H. Otsuka, A. Takahara, and K. Matyjaszewski, "Repeatable photoinduced self-healing of covalently cross-linked polymers through reshuffling of trithiocarbonate units," *Angew. Chem. Int. Ed.* **50**, 1660–1663 (2011).
- [59] South, A. B., and L. A. Lyon, "Autonomic self-healing of hydrogel thin films," *Angew. Chem. Int. Ed.* **49**, 767–771 (2010).
- [60] Ginzburg, V. V., T. Chatterjee, A. I. Nakatani, and A. K. Van Dyk, "Oscillatory and steady shear rheology of model hydrophobically modified ethoxylated urethane-thickened waterborne paints," *Langmuir* **34**, 10993–11002 (2018).
- [61] Erk, K. A., and J. F. Douglas, "Stretched exponential stress relaxation in a thermally reversible, physically associating block copolymer solution," in *MRS Online Proceedings Library Archive* **1418**, 1–8, (2012).
- [62] See supplementary material at <https://www.scitation.org/doi/suppl/10.1122/8.0000410> for supplementary figures to the article.